Article:
Amphlett, J.T.M., Ogden, M.D. orcid.org/0000-0002-1056-5799, Foster, R.I. et al. (3 more authors) (2018) Polyamine functionalised ion exchange resins: Synthesis, characterisation and uranyl uptake. Chemical Engineering Journal, 334. pp. 1361-1370. ISSN 1385-8947

https://doi.org/10.1016/j.cej.2017.11.040

Polyamine Functionalised Ion Exchange Resins: Synthesis, Characterisation and Uranyl Uptake

J. T. M. Amphlett[a], M. D. Ogden[b], R. I. Foster[a,c], N. Syna[d], K. Soldenhoff[d], *C. A. Sharrad[a]

[a] School of Chemical Engineering and Analytical Science, The University of Manchester, Oxford Road, Manchester, M13 9PL

[b] Separations and Nuclear Chemical Engineering Research (SNUCER), Department of Chemical and Biological Engineering, The University of Sheffield, Mappin Street, Sheffield, S1 3JD

[c] Decommissioning Research Technology Division, Korea Atomic Energy Research Institute, Daejeon, Republic of Korea

[d] ANSTO Minerals, Australian Nuclear Science and Technology Organisation, Locked Bag 2001, Kirrawee D. C., NSW 2232, Australia

*Corresponding author: clint.a.sharrad@manchester.ac.uk

Abstract

A series of linear polyamine functionalised weak base anion exchange resins have been synthesised using the Merrifield resin and characterised using infra-red spectroscopy, thermogravimetry, elemental analysis and solid state ^{13}C nuclear magnetic resonance spectroscopy. Uptake behaviour towards uranium (as uranyl) from sulfuric acid media has been assessed as a function of pH and sulfate concentration, with comparison to a commercially available weak base anion exchange resin, Purolite S985. Synthetic polyamine resins were seen to outperform the commercial resin at industrially relevant uranyl concentrations, with a trend of increased uptake being seen with increasing polyamine chain length. Uranium loading isotherm studies have been performed and fit with the Langmuir and Dubinin-Radushkevich isotherm models, with a maximum loading capacity observed being 269.50 mg g^{-1} for the longest polyamine chain studied. Extended X-ray absorption fine structure experiments have been used to determine uranium coordination environment on the resin surface, showing a $[UO_2(SO_4)_3]^{4-}$ species. This coordination knowledge was employed to develop an extraction mechanism and derive an isotherm model based on the law of mass action.

Keywords; Uranium, polyamine, ion exchange, EXAFS, isotherm models

1. Introduction

As of the end of 2015, there are 441 nuclear reactors in operation around the world and 68 under construction [1]. The IAEA is projecting an increase in nuclear generating capacity worldwide of up to 56% by 2030 and 135% by 2050 [1]. With this increasing global interest in nuclear power, its continued sustainability is vital to meet the energy needs of the future. Current identified uranium resources amount to 7,641,600 tU (tonnes of uranium metal), with reasonably assured resources amounting to 4,386,400 tU, an increase on 2013 values of 0.1% for identified and a decrease of 4.4% for reasonably assured resources [2]. Although these uranium resources are sufficient to meet the increasing demand, low uranium prices due to poor market conditions may make economically viable recovery difficult. This market stagnation is prompting interest in less conventional uranium sources; however, these low prices have also caused a lack of investment in the development of new uranium production technologies. This lack of development needs to be addressed, as current processing flowsheets will not be suitable for these challenging conditions [2]. The adoption of new techniques for the processing of less conventional uranium resources will result in the continued sustainability of nuclear power through a reduction in fuel cost and therefore electricity price to the public, as well as through a decreased environmental impact through extracting uranium as a co-product and from tailings.

Current uranium milling processes employ either a sulfuric acid or carbonate based system to solubilise the uranium, with the choice depending on the chemistry of the orebody [3–5]. Ideally, the chosen lixiviant would only solubilise uranium as hexavalent uranyl (UO_2^{2+}). However, due to the nature of these dissolution processes, other deleterious species in the orebody (such as Fe, Al, Mg, Mo, Mn, Ti, V, Zr) are usually dissolved into this leach liquor as well. The uranium needs to be separated from these contaminants before it can be sold as a final concentrate product for conversion, enrichment and fuel fabrication. The production of uranium from less conventional resources is highly likely to exacerbate the problem of aqueous contaminants, as the contaminant:uranium ratio will increase.

Currently, the favoured technologies for recovering uranium from the leach liquor are solvent extraction (SX) and ion exchange (IX), though there is one example of nanofiltration being used in a uranium process flowsheet [6]. For processes (i.e. *in*-situ or heap leach) where there will be a relatively low concentration of uranium, IX is the preferred technique. This can be applied as a standalone system, or as an upgrading system which can then be fed into further purification steps (e.g. SX, precipitation). Additionally, there are numerous problems associated with SX which can be overcome by using IX, such as; phase separation kinetics, solvent loss, generation of large volumes of

flammable and toxic organic waste, third phase formation and the need for an organic soluble extracting ligand [7].

The removal of uranium from sulfate media by IX typically uses anion exchange resins. This is due to the ability of uranyl ions to form anionic sulfate complexes (Eq. 1 - 3) [3,8,9] . Stability constant values for complexation reactions are given in MHL stoichiometric format where notation K indicates a stepwise equilibrium reaction while β denotes the overall equilibrium reaction. Thus a $\log_{10}\beta$ value for the complexation of x metal ions, y protons and z ligands would be denoted as $\log_{10}\beta_{xyz}$.

$$UO_2^{2+} + SO_4^{2-} \rightleftharpoons UO_2SO_4 \qquad Log_{10}\beta_{101} = 2.98 \qquad \text{Eq. 1}$$

$$UO_2^{2+} + 2\,SO_4^{2-} \rightleftharpoons [UO_2(SO_4)_2]^{2-} \qquad Log_{10}\beta_{102} = 2.83 \qquad \text{Eq. 2}$$

$$UO_2^{2+} + 3\,SO_4^{2-} \rightleftharpoons [UO_2(SO_4)_3]^{4-} \qquad Log_{10}\beta_{103} = 3.45 \qquad \text{Eq. 3}$$

There are two types of anion exchange resin, strong base and weak base. Strong base (SBA) resins contain a quaternary ammonium functional group, with an associated anionic co-ion. These are the type traditionally used in the mining industry [3,5,10]. Weak base (WBA) resins have also been shown to effectively extract uranium from sulfuric acid based milling liquors [9,11,12], but their use in uranium milling flowsheets has been limited. They can contain vinyl pyridine, polyamine and polyamide functional groups [11]. Major advantages of these WBA resins are their selectivity for uranium when compared to iron, a common and problematic contaminant element in uranium processing, and a tolerance to dissolved chloride [5,9,11–14]. Though, due to their chemical nature, these resins can only be implemented in liquors with pH 0 to pH 7 – 9, unlike SBA resins which can tolerate much more alkaline conditions (pH 0 – 13) [9]. It is noted this does give SBA resins the advantage of facile uranium elution in carbonate media. However, the advantages of SBA resins are believed to outweigh their disadvantages, with tolerance to iron and chloride in solution becoming increasingly important.

In this paper, the fundamental ion exchange characteristics of three polyamine functionalised resins towards the uptake of UO_2^{2+} in sulfate media have been explored, with comparison to a commercially available WBA resin, Purolite S985 (see Fig. 1 for functionality structures) [15]. It is hypothesised that these homologous polyamine functional groups will show an increase in uranium loading capacities with increasing chain length due to the increase in protonatable nitrogen atoms. Work has also focussed on the determination of uranium speciation on the surface of these resins, and, to the authors' knowledge, is the first paper to link a direct measurement of this to an equilibrium loading isotherm model based on the mass action law.

Additionally, this work will begin to address the lack of data in available literature with regards to uranium extraction from industrially relevant sulfate based leach liquors using WBA resins, with literature database searches for publications concerning “ion exchange”, “uranium” and “weak base” returning less than 25 outputs. This will be the first in a series of papers regarding these polyamine WBA resins, moving from initial screening and fundamental studies towards larger scale pilot plant studies utilising consecutive loading and elution cycles.

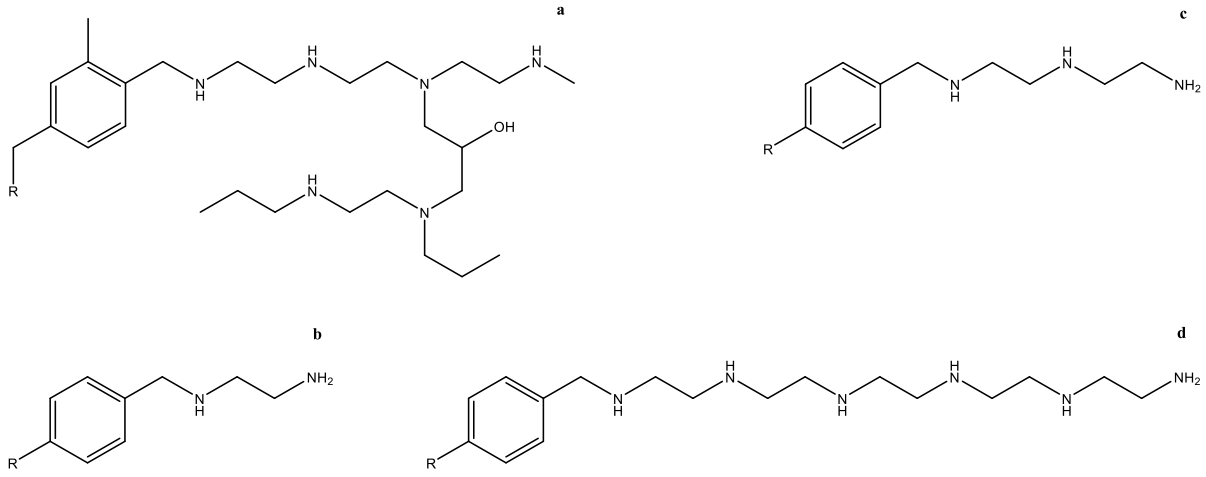

Figure 1. Resin functional groups; Purolite S985 (a), Ps-EDA (b), Ps-DETA (c), Ps-PEHA(d) **[15], R represents the resin backbone structure.**

2. Experimental

2.1. Reagents and Stock Solutions

Commercial IX resin Purolite S985 was supplied by Purolite. All reagents for resin synthesis were supplied by Sigma Aldrich and used as received. Uranium solutions for uptake and extended X-ray absorption fine structure (EXAFS) experiments were supplied by ANSTO Minerals and the University of Sheffield, respectively. All resins were preconditioned by bottle rolling with 20 bed volumes (BV) of 1 M H_2SO_4 for 24 hours and subsequently washed with 3 BV of deionised water (18 MΩ) before use.

2.2. Synthesis

Merrifield resin (40 g, 5.5 mmol g^{-1} Cl) was left to swell in 1,4-dioxane (250 mL) for 24 hours. EDA (16 g, 17.8 mL) and 1,4-dioxane (230 mL) was added to the swelled resin mixture and heated to reflux under a nitrogen atmosphere with stirring for 48 hours. The resin was removed from the 1,4-

dioxane and then washed successively with ethanol (500 mL), triethylamine (10%) in dichloromethane (300 mL), deionised water until washings reached pH 7, and ethanol (300 mL). The resultant product was Ps-EDA. Synthesis of the other resins followed the same procedure, but with different masses of the relevant amine reactant (Table 1).

Table 1. Masses of the amines EDA, DETA and PEHA used in resin synthesis.

Amine	Mass / g
Ethylenediamine (EDA)	16.00
Diethylenetriamine (DETA)	27.70
Pentaethylenehexamine (PEHA)	61.86

2.3. Characterisation

Fourier transform infra-red (FT-IR) spectroscopy was performed using a Bruker ALPHA FTIR spectrometer. Samples were prepared by grinding the resin and making a solid solution with KBr (1 wt %) followed by isostatic pressing into a pellet. FT-IR spectra of the pellets were then measured in the transmission mode. Thermogravimetric analysis was carried out using a Mettler-Toledo thermogravimetric analyser. A known mass of resin was added to a crucible and heated at a constant rate of 20 °C min^{-1} from 25 °C to 800 °C. Solid state ^{13}C NMR spectroscopy was performed on ground, dry resin samples using a Bruker BioSpin 400 MHz NMR spectrometer. Elemental analysis was carried out on a known mass of resin using a Thermo Scientific FLASH 2000 Series elemental analyser.

2.4. Uptake Studies

For both pH and sulfate dependant uptake studies, solutions containing uranium (as UO_2^{2+}) at 1 g L^{-1} were used. All experiments were performed as batch extractions by contacting 2 mL of pre-conditioned wet settled resin (WSR) with 50 mL of aqueous feed at room temperature for 24 hours on an orbital shaker. The pH range studied was from -0.5 to 6. This was adjusted using sulfuric acid, with sulfate concentration being dependent upon sulfuric acid concentration. The pH for all sample solutions was monitored using a silver/silver chloride reference electrode calibrated from pH 1-10 using buffers. At high acid concentrations ($[H^+]$ > 0.1 M), $[H^+]$ was determined by titration with standardised alkali solutions. Sulfate dependency studies were performed at a constant pH of 2, with SO_4^{2-} concentration (0 – 0.4 M) adjusted using Na_2SO_4. Extraction percentage of UO_2^{2+} was determined by the difference between the uranyl solution concentrations pre- and post-uptake,

with ion concentrations determined by ICP-MS (Perkin Elmer Elan 9000) or by ICP-OES (Perkin-Elmer Optima 5300DV).

2.5. Chloride Loading Capacity

An aqueous solution of HCl (1 M, 100 mL) was added to pre-conditioned resin (2 mL_{WSR}) and agitated for 24 hours. This process was repeated once and the resin was washed with deionised water (18 MΩ, 3 x 10 mL). The resin was then contacted with 100 mL of HNO_3 (2 M) and agitated for 24 hours. The mixture was allowed to settle and an aliquout (1 mL) of the solution phase was taken, added to deionised water (4 mL), followed by the addition of potassium chromate (5 wt%, 0.1 mL). This mixture was then titrated with a standardised aqueous solution of $AgNO_3$ until a permanent red Ag_2CrO_4 precipitate was seen.

2.6. Isotherm Studies

Loading isotherms were determined by contacting pre-conditioned resin (2 mL_{WSR}) with aqueous uranium solution (as UO_2^{2+}; up to 10 g L^{-1} U, pH 2, 50 mL) by agitation on an orbital shaker for 24 hours at room temperature. Aqueous uranium concentrations were determined pre- and post-uptake by either ICP-OES or ICP-MS. Data were fitted to derived, Langmuir (Eq. 4) and Dubinin-Radushkevich (Eq. 5) isotherm models, with fits being performed using the fitting function builder and non-linear curve fitting in Origin Pro 2015 and standard errors calculated at 95% confidence intervals:

$$q_e = \frac{bC_e q_m}{1+bC_e} \qquad \text{Eq. 4}$$

$$q_e = q_m e^{-B_{DR}\left(RTln\left(1+\frac{1}{C_e}\right)\right)^2} \qquad \text{Eq. 5}$$

where q_e is $[UO_2^{2+}]$ on the resin at equilibrium, q_m is the maximum $[UO_2^{2+}]$ loading capacity, C_e is aqueous $[UO_2^{2+}]$ at equilibrium, b is the Langmuir constant, B_{DR} is the Dubinin-Radushkevich constant, R is the universal gas constant and T is temperature. These isotherm models are commonly used to model uptake onto ion exchange resins, allowing extracted data to be compared with previously published work. It is however important to note that due to the heterovalent nature of the chemistry involved in ion exchange processes many of the underlying assumptions in the theoretical derivations of these isotherm models are violated [9,16].

2.7. EXAFS Experiments

Uranium L_{III}-edge EXAFS spectra were recorded in transmission mode on beamline B18 at the Diamond Light Source operating in a 10 min top-up mode for a ring current of 299.6 mA and an energy of 3 GeV. The radiation was monochromated with a Si(111) double crystal, and harmonic rejection was achieved through the use of two platinum-coated mirrors operating at an incidence angle of 7.0 mrad. The monochromator was calibrated using the K-edge of an yttrium foil, taking the first inflection point in the Y-edge as 17038 eV. Uptake was performed from a uranyl sulfate solution (50 mL, 1 g L^{-1}) in pH 2 H_2SO_4 using 2 mL of pre-conditioned ground resin. Sulfuric acid was used to adjust solution pH where necessary. Resin was ground prior to uptake to produce a homogenous sample and avoid packing related artifacts. Wet, dewatered resin (2 mL) was added to a cryo-tube before being vacuum sealed in plastic. The samples were left this way during measurements.

3. Results and Discussion

3.1. Resin Characterisation

3.1.1 Elemental Analysis

Elemental analysis results for chloride and nitrogen content are presented in Table 2. Theoretical nitrogen content has been calculated assuming that each polyamine chain only binds to the resin at one point, therefore only displacing one chlorine atom. The yields produced using this assumption do not agree with yields calculated from measured chlorine content in the resins. This immediately infers the presence of crosslinking via polyamine chains and their attachment to multiple benzyl groups. The amount of nitrogen in each resin increases as polyamine chain length increases, however, the overall yields decrease with increasing polyamine chain length. The yield calculated from the chlorine content does not change significantly between Ps-EDA and Ps-DETA, indicating that both EDA and DETA molecules are capable of reacting with the same amount of benzylchloride moieties. This yield is much lower for the Ps-PEHA resin. This is likely due to the relatively large size of the PEHA molecule when compared with EDA and DETA restricting the movement of it through the resin pores and reducing the amount of sites available for functionalisation. Comparing the yields calculated from the nitrogen and chlorine contents allows for the calculation of a value for the average number of bonds each polyamine chain has made to the

backbone structure of the resin. As expected, this value increases as polyamine chain length increases. These values indicate a high propensity for crosslinking with these polyamine chains.

Table 2. Elemental analysis results for nitrogen and chlorine content in the Merrifield resin, Ps-EDA, Ps-DETA and Ps-PEHA.

	Nitrogen / %			Chloride / %			Links per amine
	Theoretical	**Measured**	**Yield / %**	**Theoretical**	**Measured**	**Yield / %**	
Merrifield	0.00	0.0	-	19.5	22.7	-	-
Ps-EDA	17.90	9.82	54.9	0	2.18	90.4	1.65
Ps-DETA	26.85	11.54	43.0	0	2.41	89.4	2.08
Ps-PEHA	53.69	13.13	24.5	0	5.00	77.9	3.19

3.1.2 FT-IR Spectroscopy

Sections of the IR spectra (500 – 2000 cm^{-1}) of the Merrifield resin, Ps-EDA, Ps-DETA and Ps-PEHA are shown in Figure 2 (full spectra is available in Appendix 1, Fig.A.1, with full peak assignments given in Tables A.1, 2, 3 and 4). The spectra of the synthetic resins are very similar, though do differ from that of the Merrifield resin giving an initial qualitative insight that functionalisation was successful. The synthetic method used to functionalise the Merrifield resin with amine groups proceeds via a nucleophilic substitution reaction, with the amine replacing the chloride. Therefore, stretching frequencies in the spectra associated with alkyl chloride groups should not be observed upon functionalisation. The peak at 673 cm^{-1} in the spectrum of the Merrifield resin has been assigned to a C-Cl stretch. This peak is not present in any of the functionalised resin spectra. The Merrifield resin spectrum also shows a peak at 1265 cm^{-1}, assigned as a C-H wag in an RCH_2Cl group which is not obviously present in the spectra of the synthesised resins.

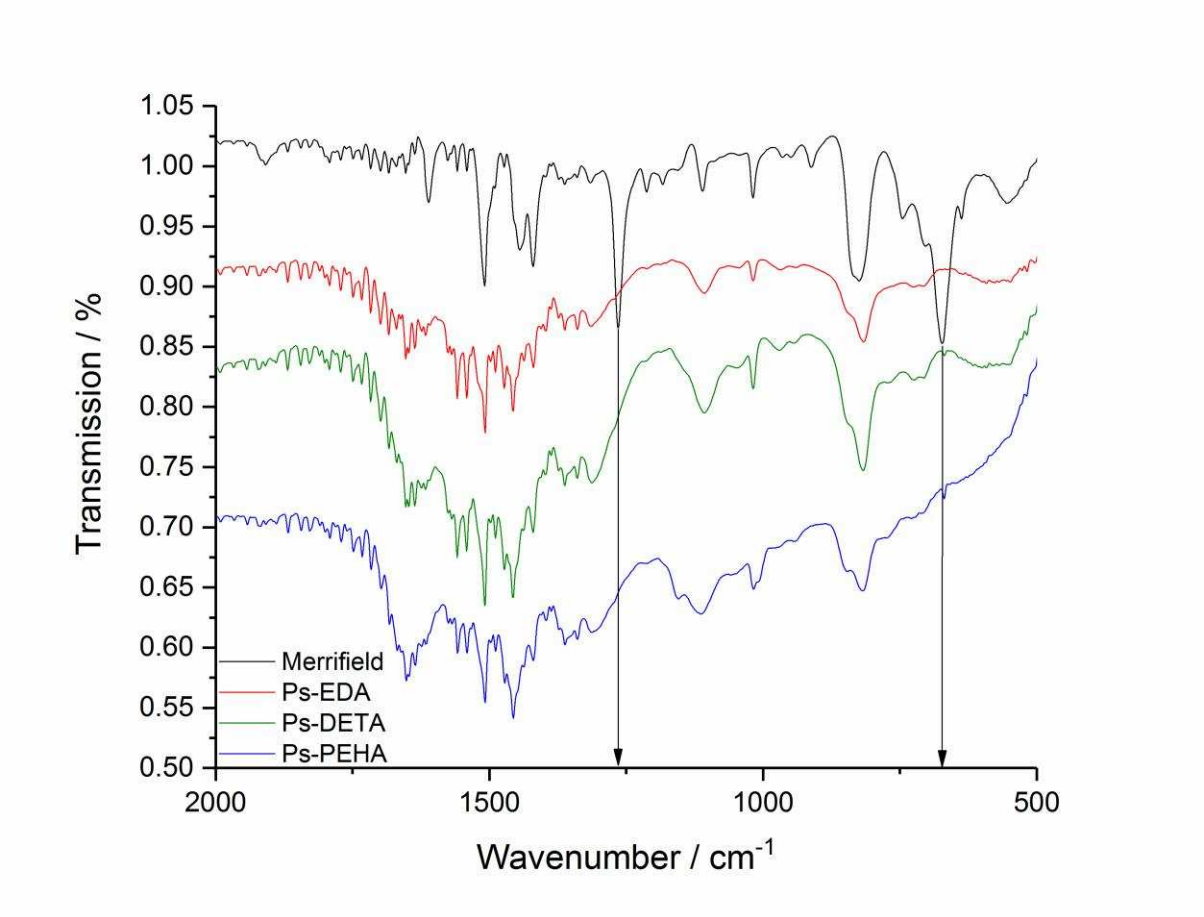

Figure 2. Section of the FT-IR spectra of the Merrifield resin, Ps-EDA, Ps-DETA and Ps-PEHA, with arrows denoting the C-Cl stretch (673 cm^{-1}) and the RCH_2Cl stretch (1265 cm^{-1}).

3.1.3 Thermogravimetric analysis

Plots of collected TGA data (Appendix 1, Fig.A.2) show a difference in the decomposition profiles of each resin. The differences observed are due to different structures of the functionality for each of the resins. There are three decomposition steps in each plot, the first of which (25 – 100 °C) relates to any residual water being driven off from the resins. Further steps pertain to the breakdown of the resin itself. The extent of mass lost during the second step (230 - 380 °C) seems to infer evidence of functionalisation. As the mass of the grafted functionality increases, so does the percentage of mass lost from the resin, as would be expected. Mass losses are detailed in Table 3. Chemical assignments of these mass losses are based on previously established studies where, during the pyrolysis of anion exchange resins, nitrogen containing species were observed to be liberated from the resin immediately above 200°C, and carbon containing species were seen to be liberated at roughly 350°C [17,18].

Table 3. Mass loss during thermogravimetric analysis of the Ps-EDA, Ps-DETA and Ps-PEHA.

	Temp. range[a] / °C	wt% lost	Degradation	Yield / %	Functionalisation / mmol g^{-1}
Ps-EDA	29 – 135	4.6	Water	33.5	1.84
	248 – 371	9.8	Polyamine/benzyl		
	371 – 655	68.4	Carbon matrix		
Ps-DETA	25 – 109	3.8	Water	29.5	1.63
	232 – 373	12.2	Polyamine/benzyl		
	373 – 686	70.5	Carbon matrix		
Ps-PEHA	26 – 112	4.8	Water	44.1	2.42
	231 – 383	27.0	Polyamine/benzyl		
	383 – 699	61.5	Carbon matrix		

[a] Temperature ranges were defined by determining the temperature where the gradient of the line deviates from that of the intermediate slope between obvious mass losses.

An initial chloride loading on the starting Merrifield Resin of 5.5 mmol g^{-1} equates to 19.5 % of the resin mass. This mass percentage should increase to 29.1, 41.3 and 61.4% for Ps-EDA, Ps-DETA and Ps-PEHA respectively. However, such a large mass loss is not observed, indicating that there is either incomplete conversion of benzylchloride groups to benzylamines, or that individual amine chains have bonded to multiple benzyl moieties. Both of those scenarios are likely as not all the chloride groups on the starting resin will be facing into the aqueous phase and able to react, as well as there being multiple nitrogen attachment sites on each amine, PEHA in particular. Attempts have been made to quantify the mass loss associated with the loss of polyamine/benzyl from TGA data (% yield, functionality per gram of resin) which will allow for calculations of uranium:functionality ratios from collected isotherm data. Calculated yields and resin functionality per gram of resin are shown in Table 3. For these calculations it has been assumed that the entire mass loss assigned to this part of the TGA profile for each resin is only associated with the polyamine chain for each resin and not any other molecular constituents of these resins, allowing for a qualitative interpretation of the TGA data. It was not possible to evaluate the species being cleaved from the resin, so it is likely that there are large errors associated with the calculated yields, due to likely complex pyrolysis mechanisms involved.

3.1.4 Solid State ^{13}C NMR Spectroscopy

Solid state (SS) ^{13}C NMR data of each of the synthesised polyamine resins and the base Merrifield resin itself are provided in Table 4, with full spectra presented in Appendix 1 (A.3, 4, 5, 6). Due to the nature of solid state NMR, and the high likelihood of crosslinking causing the formation of more complex resin functionalities, complicated spectra were obtained for the polyamine resins where full peak assignments, though attempted, must be considered tentative. In contrast, peaks in the spectrum of the Merrifield resin are assigned with much more confidence but some

discrepancies with previous work have been noted. For example, the methylene carbon atom bound to the chlorine in the Merrifield resin has been reported at both 46.2 and 40.1 ppm, with the spectrum recorded in this work having peaks at both 39.98 and 45.76 ppm [19,20]. The spectrum produced by Ansari *et*. *al*. assigns the methylene carbon to the peak at 40.1 ppm, but there is a peak slightly upfield in the spectrum which has been left unassigned. These differences in peak assignment between similar moieties illustrate the difficulty associated with this method for the characterisation of solid polymeric resins. Further to this, a spectrum of polystyrene reported by Joseph *et*. *al*. shows three peaks, at 146, 127 and 40 ppm, assigned to the quaternary aromatic carbons, protonated aromatic carbons and aliphatic carbons, respectively [21]. This would suggest that the peaks seen at 39.98 and 45.76 ppm in our Merrifield resin spectrum correspond to aliphatic carbon atoms in the polystyrene-DVB matrix and the benzylchloride methylene carbon, respectively. Our reported peaks at 127.59 and 145.29 ppm may therefore correspond to the quaternary and protonated aromatic carbons, respectively. The smaller peak at 134.60 ppm may infer the presence of sp^2 alkene carbon atoms present from unreacted divinylbenzene.

Despite the difficulties in completely assigning the SS ^{13}C NMR spectra of these resins, there are obvious qualitative differences between the Merrifield and polyamine functionalised resin spectra which must infer a difference in chemical structure, and therefore a successful functionalisation reaction. The peaks in the aromatic region of the spectrum are relatively easy to assign as they are at very similar chemical shifts to the initial resin. However, the peak assigned to unreacted divinylbenzene groups in the Merrifield resin is only seen in the DETA functionalised resin, at 137.85 ppm. This may be due to the peak being hidden in the EDA and PEHA spectra, or it could be due to different batches of Merrifield resin being used in the initial synthesis. There is much more variation seen at the downfield end of these spectra, with peaks being seen to broaden. These correspond to the polymeric matrix and the carbon atoms associated with the amine groups. An explanation for this broadening could be the effect of the protonation state of the nitrogen atoms on the amine chain on the carbon chemical shift. SS ^{13}C NMR shifts for EDA carbon atoms in the aqueous phase have been reported at 43.9 and 37.6 ppm for the unprotonated and protonated version, respectively [22]. As there are a large number of nitrogen atoms which can exchange between protonated and deprotonated forms (particularly in the PEHA resin) it is likely that the carbon atoms have unique chemical environments with subtly different chemical shifts. These slight differences in chemical shift would lead to ^{13}C NMR peak broadening and potential overlapping/obscuring of other peaks.

Table 4. Solid state ^{13}C NMR shifts and peak assignments for the Merrifield resin, Ps-EDA, Ps-DETA and Ps-PEHA.

Merrifield		Ps-EDA		Ps-DETA		Ps-PEHA	
Shift / ppm	**Assignment**	**Shift / ppm**	**Assignment**	**Shift / ppm**	**Assignment**	**Shift / ppm**	**Assignment**
39.98	Aliphatic (resin matrix)	40.45	Aliphatic (resin matrix)	41.06	Aliphatic (resin matrix)	39.87	Aliphatic (resin matrix)
45.76	Methylene (benzylchloride)	51.14	Aliphatic (benzylamino)	49.22	Aliphatic (benzylamino)	57.87	Aliphatic (benzylamino)
127.59	Quaternary aromatic	128.42	Quaternary aromatic	51.53	Aliphatic (benzylamino)	129.00	Quaternary aromatic
134.60	sp^2 alkene (divinylbenzene)	146.48	Protonated aromatic	127.59	Quaternary aromatic	146.34	Protonated aromatic
145.29	Protonated aromatic	-	-	137.85	sp^2 alkene (divinylbenzene)	-	-
-	-	-	-	143.92	Protonated aromatic	-	-

Though all the evidence (FT-IR, TGA, NMR) points towards functionalisation having taken place, it is not possible to know the exact molecular structure of the resin. It is highly likely that individual polyamine chains (DETA and PEHA in particular) will have bound to the resin at multiple sites, causing crosslinking. This could produce strong base sites, changing the character of the resin. It is believed that the functionalisation on the resin is likely to be a mixture of multiple strong and weak base functionalities. This may be advantageous, as this could convey the positive traits of SBA resins and WBA resins, such as high loading capacity and selectivity. The fully quantitative understanding of characterisation data from techniques applied to solid polymeric resins is challenging, and this work shows how important it is to use multiple techniques which can complement each other to produce a strong evidence base for proving the target product has been successfully synthesised.

3.2. Uptake Studies

3.2.1 pH and Sulfate Dependant Uptake

The uptake of uranyl by each of the polyamine resins and Purolite S985 resin from aqueous acidic sulfate media was explored using batchwise studies. All resins (2 mL_{WSR}) were able to extract over 85 % of uranyl from solutions (50 mL) with a starting uranium concentration of 1 g L^{-1} and at pH 1 – 6 ($[SO_4^{2-}] < 0.05$ M) with 24 hours of contact time at room temperature (Fig. 3). Each of the linear polyamine functionalised resins show a higher uranyl loading capacity relative to that observed from the Purolite S985 resin. No dependency on the extent of uranyl uptake with respect to pH was observed within this pH range for all studied resins. Increasing the $[H^+]$ beyond 0.1 M (pH 1) causes the uranyl uptake to decrease dramatically for all studied resins (Fig. 3).

There is a clear trend in uranyl capacity between the linear polyamine resins, which follows the increasing length of each polyamine functionality. This is suggestive of an increase in the number of sites for uptake being present with increasing nitrogen content in the functionality, but the branched functionality from the Purolite S985 does not fit with this simplistic interpretation so the overall structure of the functionality does seem to influence uptake behaviour. At $[H^+]$ concentrations above 0.3 M, the Purolite S985 resin has a higher affinity for uranyl than Ps-EDA and Ps-DETA, although it still falls behind that of the Ps-PEHA resin. This is also seen in WBA resin DOWEX M4195, where uptake suppression is seen to begin above 0.1 M H^+ in H_2SO_4 media [23]. Studies into amine functionalities grafted onto silica (aminopropylsilica, diethylenetriamine-propylsilica) showed suppression of uranyl uptake at acidic pH, with less than 50% uptake at 0.05 M H^+ (pH 3) [24].

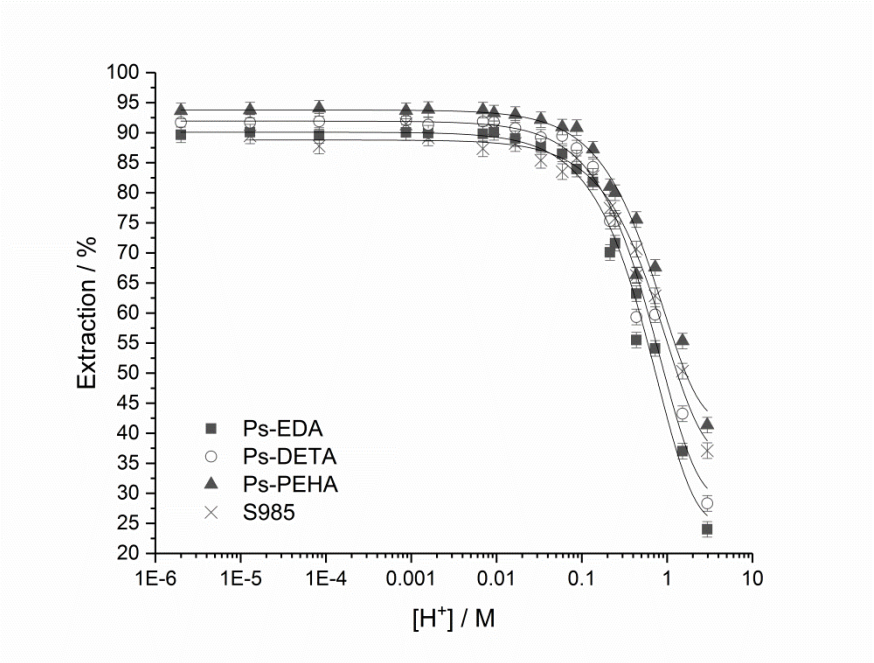

Figure 3. Extent of uranyl uptake onto Purolite S985, Ps-EDA, Ps-DETA and Ps-PEHA with respect to $[H^+]$ in sulfuric acid media ($[U]_{ini\ (aq.)}$ =1 g L^{-1}; $Vol._{(aq)}$ = 50 mL; $Vol._{WSR}$ = 2 mL) . Black line fit is presented to assist guiding the eye and error bars are ± 1 standard error.

The suppression of uranyl uptake by these resins is also seen as $[SO_4^{2-}]$ increases (Fig. 4), which agrees with previously published work on WBA resins [23]. This effect can be explained using chemical equilibria. The resins are preconditioned as the sulfate form, and it is this sulfate co-ion which is exchanging with the anionic aqueous sulfate complex. As aqueous sulfate concentration increases, the equilibrium position will tend towards the sulfate remaining on the resin, as ion exchange becomes thermodynamically less favourable. There will also be competition between anionic aqueous uranyl complexes and sulfate molecules for exchange sites on the resin. The general

trend in uranyl uptake with respect to the resins studied in this work, for the majority of the effluent conditions studied where $[H^+]$ <0. 3 M and $[SO_4^{2-}]$ > 0.1 M is as follows:

Ps-PEHA > Ps-DETA > Ps—EDA > S985.

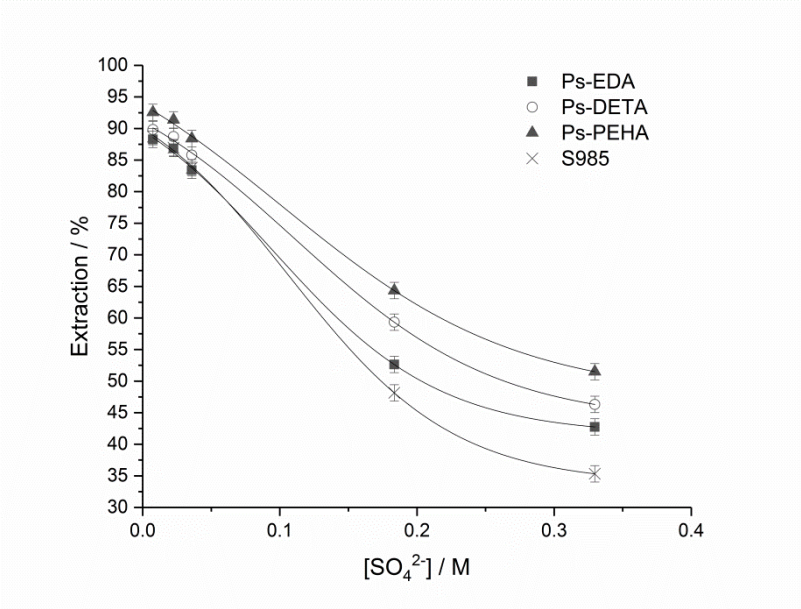

Figure 4. Uranyl uptake onto Purolite S985, Ps-EDA, Ps-DETA and Ps-PEHA at pH 2 with increasing $[SO_4^{2-}]$ (as Na_2SO_4). Black line fit is presented to assist guiding the eye and error bars are ± 1 standard error.

The strength of the interaction between the functionality and the extracted uranyl species can be assessed by looking at the pH at which 50% extraction occurs (Table 5). This "pH_{50}" can be extracted from the data by the polynomial fitting of the five closest data points to 50% uranyl extraction (R^2 > 0.9990). pH_{50} values indicate that the strength of the uptake interaction increases as the polyamine chain length increases. However, this does not hold true for the Purolite S985 resin, as it has the second highest pH_{50} but the lowest extraction percentage.

Table 5. pH_{50} and $[H^+]_{50}$ values for Purolite S985, Ps-EDA, Ps-DETA and Ps-PEHA.

Resin	# N atoms	pH_{50}	$[H^+]_{50}$ / M	$p[SO_4^{2-}]_{50}$	$[SO_4^{2-}]_{50}$ / M
Ps-EDA	2	0.064	0.862	0.680	0.209
Ps-DETA	3	-0.089	1.227	0.562	0.274
Ps-PEHA	6	-0.293	1.963	0.446	0.358
Purolite S985	6	-0.185	1.532	0.754	0.176

3.3. EXAFS Experiments

Multiple EXAFS data sets were collected for each resin. These were then combined and normalised using the Athena software package [25]. These spectra were then processed and fits were performed using the FEFF database via the software package Artemis [25,26]. There is little visual difference between the spectra, alluding to the same uranium environment and uptake mechanism for all resins (Fig. 5). Fits were attempted using crystallographic data from the inorganic crystal structure database (ICSD) [27,28]. A chelation model was initially attempted with the functional groups being multidentate with respect to the uranyl ion, however these did not give statistically justifiable fits. When a uranyl species corresponding to an anion exchange mechanism was fit, statistical parameters were acceptable. The fitted species is 6-coordinate in the equatorial plane, with three bidentate sulfate groups ($[UO_2(SO_4)_3]^{4-}$), using a Hanning window with r_{min} = 1 Å and r_{max} = 4 Å (Fig. 6). The U-S interatomic distances (Table 6) indicate a bidentate as opposed monodentate sulfate group [29]. Fitting paths included one axial oxygen environment (n = 2), two equatorial oxygen environments (n = 2, 4), two equatorial sulfate environments (n = 1, 2) and two multiple scattering paths. The number of variables fit never exceeded two thirds of the independent points available for each data set. This species fits with data collected for maximum resin capacity measured by chloride uptake, as $[UO_2^{2+}]_{max}/[Cl^-]_{max} \approx 4$ (Table 7), indicating an anionic uranyl species with -4 charge that interacts with the resins.

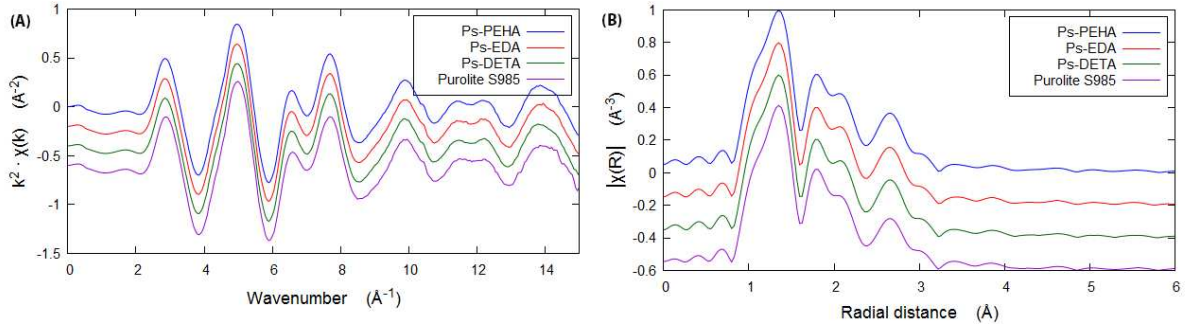

Figure 5. (A) The U L_{III}-edge k^2-weighted EXAFS spectra and (B) the corresponding Fourier transforms (R-space) for uranyl on Purolite S985, Ps-EDA, Ps-DETA and Ps-PEHA.

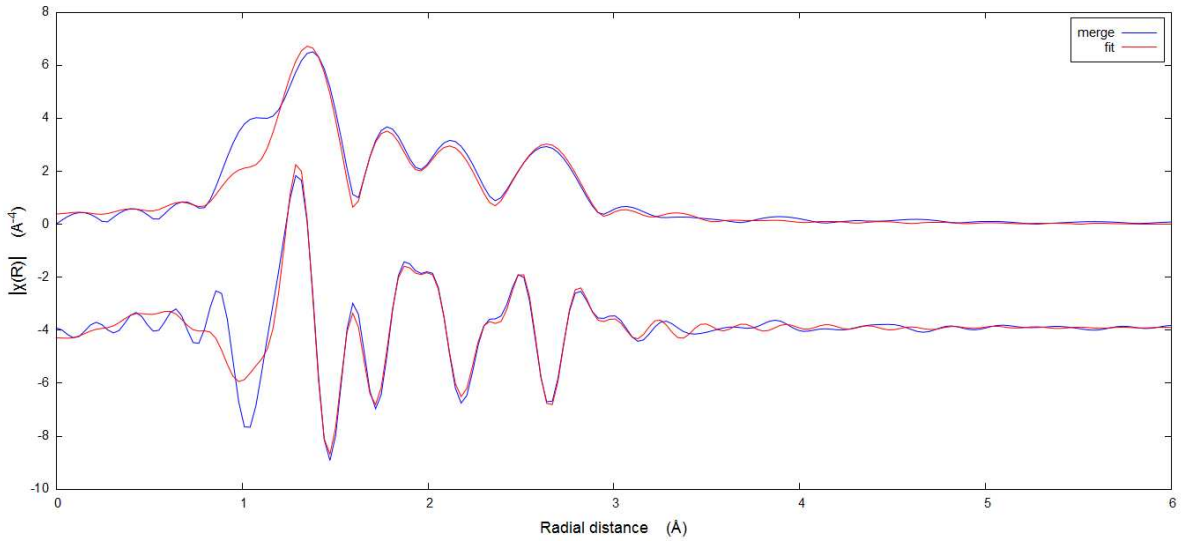

Figure 6. U L_{III}-edge EXAFS spectrum in R-space (above) and k-space (below) for the uptake of $[UO_2(SO_4)_3]^{4-}$ onto synthetic resin Ps-PEHA. Spectra for other resins can be found in Appendix 1 (A.7, 8, 9).

Table 6. U L_{III}-edge EXAFS data.

	Scattering path	n[a]	Interatomic Distances / Å	σ^{2} [b]	R-factor[c]
Purolite S985	U - O_{axial}	2	1.79	0.00221	0.0183
	U - $O_{equatorial}$	4	2.48	0.00488	
	U - $O_{equatorial}$	2	2.33	0.00358	
	U - S	2	3.11	0.00211	
	U - S	1	3.24	0.00176	
Ps-EDA	U - O_{axial}	2	1.79	0.00219	0.0204
	U - $O_{equatorial}$	4	2.48	0.00444	
	U - $O_{equatorial}$	2	2.34	0.00356	
	U - S	2	3.11	0.00149	
	U - S	1	3.24	0.00108	
Ps-DETA	U - O_{axial}	2	1.79	0.00216	0.0213
	U - $O_{equatorial}$	4	2.45	0.00444	
	U - $O_{equatorial}$	2	2.34	0.00337	
	U - S	2	3.11	0.00154	
	U - S	1	3.24	0.00127	
Ps-PEHA	U - O_{axial}	2	1.79	0.00230	0.0204
	U - $O_{equatorial}$	4	2.48	0.00445	
	U - $O_{equatorial}$	2	2.34	0.00356	
	U - S	2	3.11	0.00147	
	U - S	1	3.24	0.00115	

[a]Number of occupants fixed. [b]Debye-Waller factor. [c]Parameter describing the goodness of fit.

Table 7. The ratio of maximum uranyl capacity to maximum chloride capacity for Ps-EDA, Ps-DETA and Ps-PEHA, determined by chloride titration.

Resin	$[UO_2^{2+}]_{max}$ / $[Cl^-]_{max}$
Ps-EDA	4.886
Ps-DETA	4.335
Ps-PEHA	4.068

3.4 Isotherm Modelling Studies

3.4.1 Langmuir and Dubinin-Raduchkevich

Isotherm data were fitted using both the Langmuir and Dubinin-Radushkevich isotherms; with the goodness of fit parameter (R^2) indicating a better fit was obtained with the Langmuir model (Fig. 7, Tables 8 and 9). The trend in uptake capacity at low uranyl concentration is consistent with pH and [SO_4^{2-}] screening studies. However, at higher [UO_2^{2+}] concentrations, the uranyl capacity of Purolite S985 surpasses that of the synthetic polyamine resins. These high concentrations are unrealistic when compared with those found in real mining circuits. The Dubinin-Radushkevich isotherm model allows for the calculation of the mean free energy of sorption, where a value below 8 kJ mol^{-1} corresponds to a physisorption uptake mechanism, and one above corresponding to a chemisorption uptake mechanism [23]. Although this isotherm model does not describe uptake behaviour as well as the Langmuir, the mean free energy of sorption values obtained would suggest a chemisorption mechanism, which agrees with an ion exchange system.

Table 8. Fitting parameters for Purolite S985, Ps-EDA, Ps-DETA and Ps-PEHA fit with the Langmuir isotherm model.

	Ps-EDA	**Ps-DETA**	**Ps-PEHA**	**S985**
q_m / mg g^{-1}	176.55 ± 2.51	195.47 ± 4.23	252.28 ± 4.46	283.22 ± 5.74
q_m (x10^{-3}) / mol g^{-1}	0.742 ± 0.011	0.821 ± 0.018	1.060 ± 0.019	1.190 ± 0.024
b (x10^3)	1.097 ± 0.054	1.042 ± 0.080	1.397 ± 0.088	0.519 ± 0.036
R^2	0.997	0.993	0.995	0.996

Table 9. Fitting parameters for Purolite S985, Ps-EDA, Ps-DETA and Ps-PEHA fit with the Dubinin-Radushkevich isotherm model.

	Ps-EDA	**Ps-DETA**	**Ps-PEHA**	**S985**
q_m / mg g^{-1}	261.8 ± 14.87	295.12 ± 12.99	378.42 ± 18.69	480.76 ± 24.15
q_m (x10^{-3}) / mol g^{-1}	1.100 ± 0.062	1.240 ± 0.055	1.590 ± 0.079	2.020 ± 0.101
B_{DR} (x 10^{-9})	4.26 ± 0.28	4.40 ± 0.22	4.09 ± 0.23	5.81 ± 0.29
E / kJ mol^{-1}	10.84 ± 0.35	10.66 ± 0.27	11.06 ± 0.32	9.28 ± 0.23
R^2	0.971	0.983	0.978	0.986

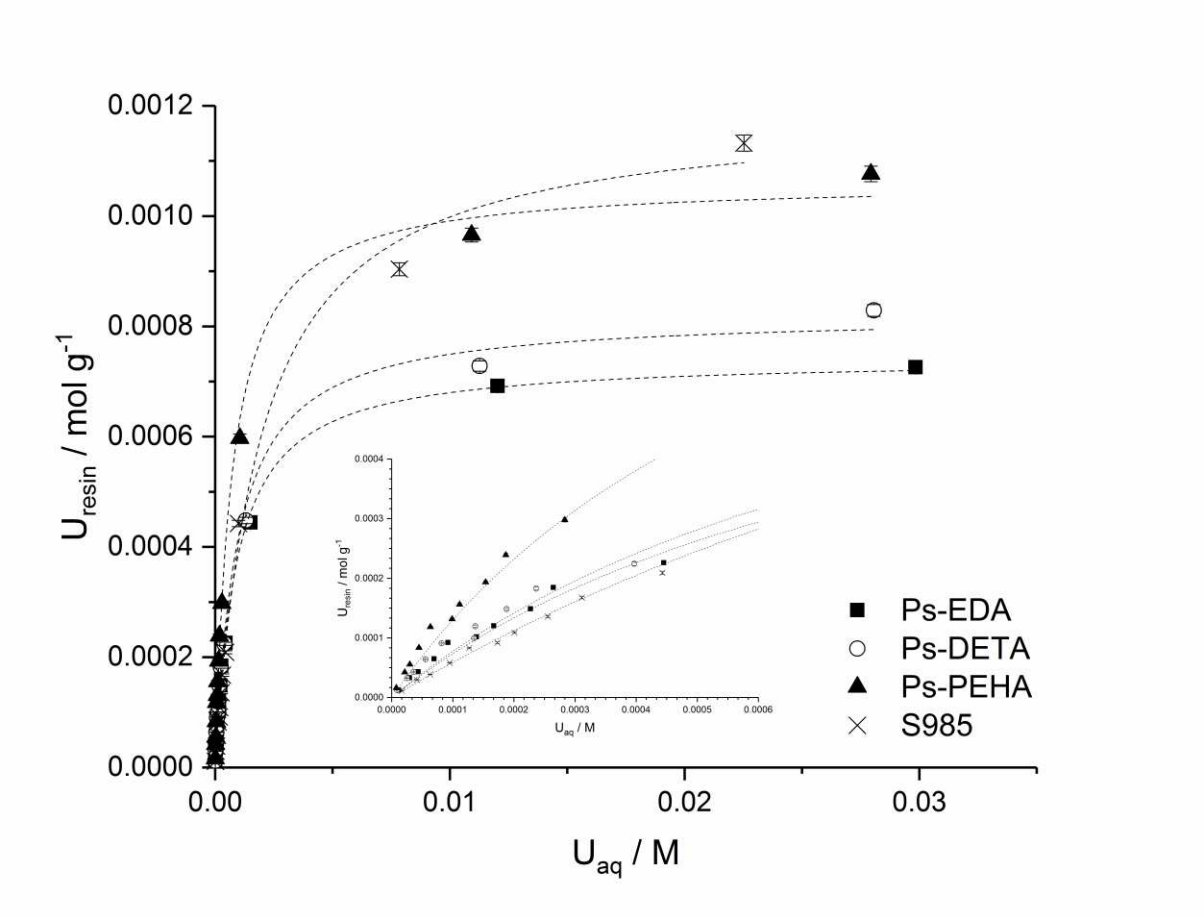

Figure 7. Langmuir fits of isotherm data collected for Purolite S985, Ps-EDA, Ps-DETA and Ps-PEHA. The Langmuir model fit for each resin is shown by a dashed line.

3.4.2 Derived Isotherm

Based on EXAFS experimental fits and chloride titration data, an isotherm model has been derived. This isotherm is based on the equilibrium of two fully protonated $[EDA(H)_2]^{2+}$ functionalities exchanging four bound $[HSO_4]^-$ with one $[UO_2(SO_4)_3]^{4-}$ species on the resin amine active site (Eq. 6). This equilibrium allows for the derivation of an isotherm model representative of this IX system based on the law of mass action (Eq. 7), where $y=[UO_2]_{resin}$, $S=[UO_2]_{resin,max}$, $x=[UO_2]_{aq}$ and K_{ex}'=an effective equilibrium constant (full derivation is available in Appendix 2). Experimental fits are presented in Figure 8. Goodness of fit parameters (Table 10) suggest that this model fits the collected data better than both the Langmuir and the Dubinin-Radushkevich isotherms.

$$\overline{2[RN_2H_2(HSO_4)_2]} + [UO_2(SO_4)_3^{4-}] \rightleftharpoons \overline{[(RN_2H_2)_2(UO_2(SO_4)_3)]} + 4[HSO_4^-] \qquad \text{Eq. 6}$$

$$y = \frac{(4K'_{ex}xS+1) \pm \sqrt{(-4K'_{ex}xS+1)-(4K'_{ex}xS)^2}}{8K'_{ex}x} \qquad \text{Eq. 7}$$

Table 10. Fitting parameters for Ps-EDA, Ps-DETA, Ps-PEHA and Purolite S985 fit with the derived isotherm model.

	Ps-EDA	Ps-DETA	Ps-PEHA	S985
S / mg g^{-1}	209.44 ± 6.75	233.24 ± 6.31	297.50 ± 5.67	365.33 ± 14.81
q_m (x10^{-3}) / mol g^{-1}	1.760 ± 0.028	1.960 ± 0.027	2.500 ± 0.024	3.070 ± 0.062
K_{ex}' (x10^5)	3.382 ± 0.239	2.837 ± 0.170	3.061 ± 0.132	0.755 ± 0.063
R^2	0.997	0.998	0.999	0.997

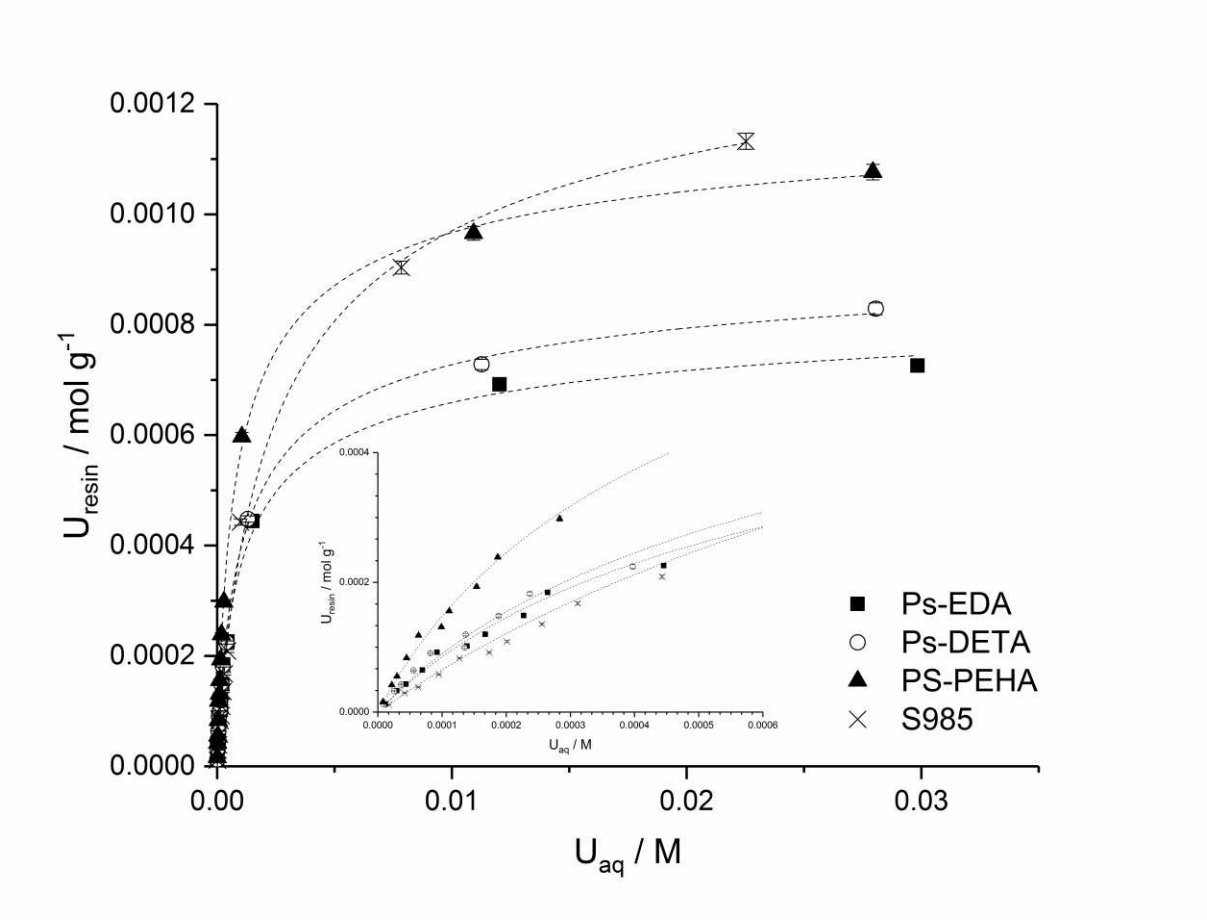

Figure 8. Fitting of the derived isotherm to data collected for uranyl uptake onto Ps-EDA, Ps-DETA and Ps-PEHA and Purolite S985. Speciation based isotherm model shown by dashed line fits.

Though the model fits with the data, it is likely to be a simplification of a complex mechanism, potentially involving other uranyl species on the surface of the resin and in the bulk solution. Even if in the bulk solution there are lower sulfated uranyl species (e.g. $[UO_2(H_2O)_x(SO_4)_y]$ where y < 3) present, the expected high sulfate concentration within the immediate environment of the sulfuric acid washed resins will most likely cause a change in any such uranyl species that approaches these resins to the tris(sulfato) uranyl complex. As discussed previously, there may be strong base sites produced from the crosslinking of amine chains and even unprotonated nitrogen atoms which could interact directly with bound uranyl, potentially introducing a degree of chelation to the mechanism. This could infer a degree of tolerance to high ionic strength (*e.g.* high Cl^- in

seawater) which would be advantageous for these resins over traditional strong base resins. EXAFS is a bulk technique giving an average of all species present, so the existence of a chelated species on the resin cannot be ruled out completely. However, results do seem to suggest that the dominant species on the surface of the resin is $[UO_2(SO_4)_3]^{4-}$, which gives confidence that this isotherm is representative of uranyl speciation on these weak base anion exchange resins.

Observed maximum loading capacities for the Ps-EDA, Ps-DETA, Ps-PEHA and Purolite S985 are 172.73, 197.30, 256.21 and 269.50 mg g^{-1} respectively, which were achieved from a 10 g L^{-1} uranium solution. These values are predicted most effectively by the derived isotherm model, with the Langmuir model, though fitting adequately, overestimates these values. WBA resin DOWEX M4195 has been predicted to have a maximum loading capacity of 78 mg g^{-1} from Langmuir model fits [23]. Anion exchange resin Amberlite CG-400 has shown predicted uptake capacities of 112.36 mg g^{-1} [30], with values for a ethylenediamine-tris(methylenephosphonic) acid resin being 64.26 mg g^{-1} [31]. This shows the potential of these resins to outperform similar commercially available WBA resins and ones with novel functionalities synthesised in academia (Table 11).

Table 11. Maximum uranyl capacities for a selection of ion exchange resins

Extractant	q_m (UO_2^{2+}) / mg g_r^{-1}	Aqueous Medium
Ps-EDA	172.73	pH 2 H_2SO_4
Ps-DETA	197.30	pH 2 H_2SO_4
Ps-PEHA	256.21	pH 2 H_2SO_4
Purolite S985	269.50	pH 2 H_2SO_4
Dowex M4195 [23]	78	pH 1.7 H_2SO_4
Amberlite CG-400 [30]	112.36	pH 3.5 HCl in the presence of PO_4^{3-}
Polystyrene/Divinylbenzene functionalised with ethylenediaminetris(methylenephosphonic) acid [32]	41.76	pH 3.4 nitric acid
Glycidylmethacrylate/Divinylbenzene functionalised with pentaethylenehexamine [33]	129.87	pH 4.5 nitric acid
Polystyrene/Divinylbenzene functionalised with N,N'-dimethyl-N,N'-dibutylmalonamide [20]	18.78	3 M HNO_3
Amberlite XAD-4 functionalised with succinic acid [34]	12.33	pH 4.5 Hexamine-HCl buffer
Polyethyleniminephenylphosphonamidic acid [35]	39.66	Nitric acid, concentration not given

The maximum uranium loading capacities predicted by the model fit can be used alongside the estimated amount of functionality per gram of resin (Table 3) to calculate uranium:functionality molar ratios and subsequently the uranium:nitrogen atomic ratios (Table 12). If it is assumed that all

the amine groups exist in the protonated form and no other ions apart from $[UO_2(SO_4)_3]^{4-}$ are present in the immediate binding sphere, the expected average uranium:functionality ratios would be 0.50, 0.75 and 1.50 for Ps-EDA, Ps-DETA and Ps-PEHA, respectively, in order to maintain charge balance. Despite the unlikely assumption that all the amine groups present on the resin are protonated, these ratios indicate that there is more uranium present on the loaded Ps-EDA and Ps-DETA resins than would be expected. We believe that the most likely reasoning for this is the use of the TGA data is underestimating the total amount of functionality that is present on the resin. The maximum chloride loading capacity for each resin falls within 4-5 times of the respective uranyl capacity indicating the discrepancies in the uranyl:functionality ratios are unlikely to be due to errors in determining the uranium capacities. The most likely explanation for the underestimation of the functionality on the resins is the simplistic assumption that only the polyamine functionality is cleaved during thermal degradation process is not valid. There is also the possibility that cross-linked polyamine functionality groups do not degrade from the resin as readily as those attached at a single site. This shows that the observed mass losses cannot be directly prescribed to the loss of a specific functionality using TGA data alone and can only be used for a qualitative understanding under the conditions studied. The combination of TGA with gas chromatography or mass spectrometry could allow for an improved quantitative analysis. Repeating this process with collected elemental analysis data (Table 2) produces uranium:functionality and uranium:nitrogen ratios which closely agree with maximum loading capacities (Table 12).

Table 12. Calculated ratios of uranium:functionality (molar) and uranium:nitrogen (atomic) calculated by various means using TGA and elemental analysis data for Ps-EDA, Ps-DETA and Ps-PEHA

	Uranium:Functionality			**Uranium:Nitrogen**		
	Calculated theoretical average[a]	**Experimental calculation (TGA)[b]**	**Experimental calculation (EA)[c]**	**Calculated theoretical average[a]**	**Experimental calculation (TGA)[b]**	**Experimental calculation (EA)[c]**
Ps-EDA	0.50	0.95	0.50	0.25	0.48	0.25
Ps-DETA	0.75	1.21	0.71	0.25	0.40	0.24
Ps-PEHA	1.50	1.03	1.60	0.25	0.17	0.27

[a] Calculated by assuming charge balance is maintained in the immediate binding sphere, all amine groups are protonated and no other ions, apart from $[UO_2(SO_3)]^{4-}$, are present in the immediate binding sphere.

[b] Calculated using the uranium loading estimated from derived model isotherm fits and the quantity of functionality loading estimated from TGA data.

[c] Calculated using the uranium loading estimated from derived model isotherm fits and the quantity of functionality loading calculated from elemental analysis data.

4. Conclusions

The three synthetic resins (Ps-EDA, Ps-DETA and Ps-PEHA) have been successfully synthesised as evidenced by the characterisation techniques employed. The Merrifield resin has been shown to be an effective starting material from which to produce IX resins as the chloride leaving group is able to participate readily in nucleophilic substitution reactions.

All synthetic resins were effective in removing uranyl from aqueous sulfate media, with maximum uranyl loading capacities of 172.73, 197.30, 256.21 mg g_{wsr}^{-1} observed for Ps-EDA, Ps-DETA and Ps-PEHA, respectively. All synthetic resins outperformed the commercial resin Purolite S985 at industrial process (i.e. *in*-situ or heap leach) uranyl concentrations (Table 14) but show lower q_m values at higher initial uranium concentrations. This suggests that Purolite S985 may be better suited for uranium recovery from dynamic leach process liquors with higher uranyl concentrations [36]. It is difficult to directly compare these results with those from other previously reported studies of uranyl extraction by ion exchange resins due to the wide range of aqueous conditions used across these investigations. Additionally, many of the uranyl maximum loading capacities reported are predicted from isotherm models, not experimentally measured values.

Table 14. Constituents of a process water provided to the authors by ANSTO Minerals

Species	Concentration / mg L^{-1}
K^+	128
Na^+	107
Ca^{2+}	495
Mg^{2+}	5677
Mn^{2+}	2110
UO_2^{2+}	25
Al^{3+}	291
Fe^{3+}	< 1
SO_4^{2-}	12462
PO_4^{3-}	6
SiO_4^{4-}	31

EXAFS experiments suggested that the synthetic resins all follow a relatively simple ion exchange mechanism, with $[UO_2(SO_4)_3]^{4-}$ being extracted onto the resin. This mechanism fits the collected isotherm data well, with calculated maximum uranium loading capacities from these fits agreeing well with experimentally determined values.

These resins are promising candidates for further research towards their use in uranium mining flowsheets. Future work with these resins will involve assessing their tolerance to common contaminant species in uranium mining process waters, as well as the effects of Fe^{3+} and Cl^- to assess the potential application of these resins for the extraction of uranium from low quality ores

and waters, respectively. Determination of uranium extraction properties under continuous flow column loading will be carried out in small scale laboratory experiments before scaling up to pilot plant studies with multiple extraction/elution cycles. These studies will be presented in future publications.

5. Acknowledgements

This work was funded by the UK Engineering and Physical Sciences Research Council (EPSRC reference: EP/G037140/1). The authors would like to thank the Diamond Light Source for access to beamline B18 (SP12643-1), especially Dr. Stephen Parry and Dr. Giannantonio Cibin for their assistance with data acquisition, as well as Prof. Kath Morris for her help with sample preparation. We thank ANSTO Minerals for hosting Mr. James Amphlett for a six month research visit, providing expertise, aqueous uranium samples and access to analytical services. We also thank Dr. Barbara Gore for her invaluable assistance with running SS ^{13}C NMR experiments at the NMR service in the School of Chemistry at The University of Manchester.

6. References

[1] IAEA, Energy, Electricity and Nuclear Power Estimates for the Period up to 2050, Vienna, 2016.

[2] Nuclear Energy Agency and International Atomic Energy Agency, Uranium 2016: Resources, Production and Demand, 2016. doi:https://www.oecd-nea.org/ndd/pubs/2004/5291-uranium-2003.pdf.

[3] C.R. Edwards, A.J. Oliver, Uranium processing: A review of current methods and technology, J. Miner. Met. Mater. Soc. 52 (2000) 12–20. doi:10.1007/s11837-000-0181-2.

[4] M.A. Ford, Uranium in South Africa, J. South African Inst. Min. Metall. 93 (1993) 37–58. doi:10.1111/j.1813-6982.1953.tb01589.x.

[5] A. Taylor, Short Course in Uranium Ore Processing, Short Course Uranium Ore Process. (2016).

[6] M. Peacock, S. McDougall, P. Boshoff, D. Butcher, M. Ford, S. Donegan, D. Bukunkwe, Nano-filtration technology for reagent recovery, in: ALTA Uranium-REE Sess., ALTA Metallurgical Services Publications, Perth, 2016.

[7] J. Veliscek-Carolan, Separation of actinides from spent nuclear fuel: A review, J. Hazard. Mater. 318 (2016) 266–281. doi:10.1016/j.jhazmat.2016.07.027.

[8] E.J. Zaganiaris, Ion Exchange Resins in Uranium Hydrometallurgy, Books on Demand France, 2009.

[9] E.M. Moon, M.D. Ogden, C.S. Griffith, A. Wilson, J.P. Mata, Impact of chloride on uranium(VI) speciation in acidic sulfate ion exchange systems: Towards seawater-tolerant mineral processing circuits, J. Ind. Eng. Chem. 51 (2017) 255–263. doi:10.1016/j.jiec.2017.03.009.

[10] International Atomic Energy Agency, Uranium Extraction Technology, Tech. Reports Ser. 359. (1993) 183.

[11] F.X. Mcgarvey, J. Ungar, The influence of resin functional group on the ion-exchange recovery of uranium, J. South. African Inst. Min. Metall. 81 (1981) 93–100.

[12] R. Kunin, R.L. Gustafson, E.G. Isacoff, H.F. Fillius, Ion Exchange Resins for Uranium Hydrometallurgy, Eng. Min. J. 170 (1969) 73–79.
[13] A. Rezkallah, J.F. Ferraro, P.M. Pellny, Removal of Uranium from Water, WO2014126699 A1, 2014.
[14] Boss Resources Limited, Boss Receives Positive Resin Test Results In Expansion Study, (2016).
[15] A.N. Nikoloski, K.L. Ang, D. Li, Recovery of platinum, palladium and rhodium from acidic chloride leach solution using ion exchange resins, Hydrometallurgy. 152 (2015) 20–32. doi:10.1016/j.hydromet.2014.12.006.
[16] M.A. Fernandez, G. Carta, Characterization of protein adsorption by composite silica-polyacrylamide gel anion exchangers. I. Equilibrium and mass transfer in agitated contactors, J. Chromatogr. A. 746 (1996) 169–183. doi:10.1016/0021-9673(96)00337-8.
[17] U. Chun, Pyrolysis and Oxidative Pyrolysis Experiments with Organic Ion Exchange Resins, Daejon, Republic of Korea, n.d.
[18] M. Matsuda, K. Funabashi, T. Nishi, H. Yusa, M. Kikuchi, Decomposition of Ion Exchange Resins by Pyrolysis, Nucl. Technol. 75 (1986) 187.
[19] J. Elguero, R.M. Claramunt, R. Garceran, S. Julia, M. Avila, J.M. del Mazo, 13C NMR Study of Polyphenyl-, Poly-N-azolyl- and Poly-N- benzazoyl-methanes, Magn. Reson. Chem. 25 (1987) 260–268.
[20] S. A. Ansari, P.K. Mohapatra, V.K. Manchanda, Synthesis of N,N'-dimethyl-N,N'-dibutyl malonamide functionalized polymer and its sorption affinities towards U(VI) and Th(IV) ions, Talanta. 73 (2007) 878–885. doi:10.1016/j.talanta.2007.05.007.
[21] R. Joseph, W.T. Ford, S. Zhang, M.P. Tsyurupa, A. V Pastukhov, V.A. Davankov, Solid-State 13C-NMR Analysis of Hypercrosslinked Polystyrene, J. Polym. Sci. Part A Polym. Chem. 35 (1996) 695–701. doi:10.1002/(SICI)1099-0518(199703)35:4<695::AID-POLA12>3.0.CO;2-I.
[22] S.P. Dagnall, D.N. Hague, M.E. McAdam, 13C nuclear magnetic resonance study of the protonation sequence of some linear aliphatic polyamines, J. Chem. Soc. Perkin Trans. 2. (1984) 1111. doi:10.1039/p29840001111.
[23] M.D. Ogden, E.M. Moon, A. Wilson, S.E. Pepper, Application of chelating weak base resin Dowex M4195 to the recovery of uranium from mixed sulfate/chloride media, Chem. Eng. J. 317 (2017) 80–89. doi:10.1016/j.cej.2017.02.041.
[24] X. Sun, P.L. Zanonato, D. Bernardo, Z. Zhang, L. Rao, P. Di Bernardo, Sorption of Uranium and other Metal Ions on Amine-Functionalized Silica Materials Sorption of Uranium and other Metal Ions on Amine-Functionalized Silica Materials, Sep. Sci. Technol. 5018 (2015) 2769–2775. doi:10.1080/01496395.2015.1085403.
[25] B. Ravel, M. Newville, *ATHENA* , *ARTEMIS* , *HEPHAESTUS* : data analysis for X-ray absorption spectroscopy using *IFEFFIT*, J. Synchrotron Radiat. 12 (2005) 537–541. doi:10.1107/S0909049505012719.
[26] M. Newville, IFEFFIT : interactive XAFS analysis and FEFF fitting, J. Synchrotron Radiat. 8 (2001) 322–324.
[27] M.B. Doran, A.J. Norquist, D. O 'Hare, Exploration of Composition Space in Templated Uranium Sulfates, Inorg. Chem. 42 (2003) 6989–6995. doi:10.1021/ic034540j.
[28] F.W. Lewis, L.M. Harwood, M.J. Hudson, M.G.B. Drew, M. Sypula, G. Modolo, D. Whittaker, C.A. Sharrad, V. Videva, V. Hubscher-Bruder, F. Arnaud-Neu, Complexation of lanthanides, actinides and transition metal cations with a 6-(1,2,4-triazin-3-yl)-2,2':6',2''-terpyridine ligand: implications for actinide (III)/lanthanide(III) partitioning, Dalt. Trans. 41 (2012) 9209. doi:10.1039/c2dt30522d.
[29] C. Hennig, K. Schmeide, V. Brendler, H. Moll, S. Tsushima, A.C. Scheinost, The Structure of Uranyl Sulfate in Aqueous Solution - Monodentate Versus Bidentate Coordination, in: 13th Int. Proc. X-Ray Absorpt. Fine Struct., 2006: pp. 262–264.
[30] F. Semnani, Z. Asadi, M. Samadfam, H. Sepehrian, Uranium(VI) sorption behavior onto amberlite CG-400 anion exchange resin: Effects of pH, contact time, temperature and

presence of phosphate, Ann. Nucl. Energy. 48 (2012) 21–24. doi:10.1016/j.anucene.2012.05.010.
[31] V.K. Jain, A. Handa, S.S. Sait, P. Shrivastav, Y.K. Agarval, Preconcentration, separation and trace determination of lanthanum (III), cerium (III), thorium (IV) and uranium (VI) on polymer supported ovanillinsemicarbazone, Anal. Chim. Acta. 429 (2001) 237–246.
[32] A. Kadous, M.A. Didi, D. Villemin, A new sorbent for uranium extraction: Ethylenediamino tris(methylenephosphonic) acid grafted on polystyrene resin, J. Radioanal. Nucl. Chem. 284 (2010) 431–438. doi:10.1007/s10967-010-0495-7.
[33] S.A. Sadeek, E.M.M. Moussa, M.A. El-Sayed, M.M. Amine, M.O. Abd El-Magied, Uranium(VI) and Thorium(IV) Adsorption Studies on Chelating Resin Containing Pentaethylenehexamine as a Functional Group, J. Dispers. Sci. Technol. 35 (2014) 926–933. doi:10.1080/01932691.2013.809507.
[34] P. Metilda, K. Sanghamitra, J. Mary Gladis, G.R.K. Naidu, T. Prasada Rao, Amberlite XAD-4 functionalized with succinic acid for the solid phase extractive preconcentration and separation of uranium(VI), Talanta. 65 (2005) 192–200. doi:10.1016/j.talanta.2004.06.005.
[35] O. Abderrahim, M.A. Didi, D. Villemin, A new sorbent for uranium extraction: Polyethyleniminephenylphosphonamidic acid, J. Radioanal. Nucl. Chem. 279 (2009) 237–244. doi:10.1007/s10967-007-7270-z.
[36] D. Van Tonder, M. Kotze, Uranium recovery from acid leach liquors: IX or SX?, in: Alta 2007 Uranium Conf. Proc., 2007.